Small bodies of the solar system

Lecture by Klaus Jockers, Göttingen, winter term 2004/2005

Comets3

Cometary Dust

Cometary dust

Why to study cometary dust?

• Cometary dust comprises as much or possibly more of the cometary mass than cometary gas and plasma, therefore, if we want to know the chemical composition of comets we must know the chemical composition of the dust.
• The dust may differ in different comets like the surfaces of different asteroids.
• In the interstellar medium dust is the catalyst for complicated molecules. Cometary dust carries organic substances important for the creation of complicated molecules, perhaps even of life.

Methods to study cometary dust

- Mie theory of light scattering by spherical particles
- Motion of cometary dust particles under the influence of solar radiation pressure
- Brightness and polarization of cometary dust grains and its phase dependence
- Thermal radiation of dust and grain albedo
- Silicate emission in the 9-14 μm wavelength range
- Overheat effect of small grains
- Color of cometary dust
- Space observations of comets 1P/Halley and 81P/Wild 2
  a: particle counters
  b: measuring the composition of cometary grains in situ.

Mie theory is the theory of light scattering by spherical particles, developed in the beginning of 20th century. It is so far the only simple way to study the light scattering of any particle.

κ imaginary part of refractive index, "absorption index"

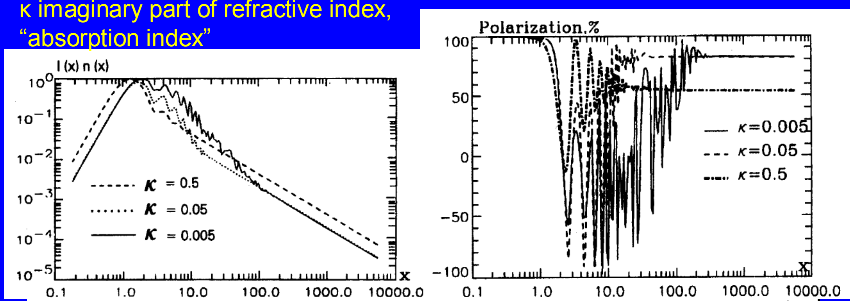

Figure 2. Light scattered by spherical particles having a power law size distribution with index $a = 3$ observed at phase angle $\alpha = 90°$. (a) Relative intensity versus size parameter x. (b) Polarization versus size parameter x for an individual particle.

Size parameter $x = 2\pi r/\lambda$. For λ = 0.628 μm $r = x/10$.
For a power index of 3.0 particles of radius 0.2 μm contribute most to the scattered light.
Polarization increases with absorption index "Umov's law" , but otherwise is not realistic for cometary dust particles.

Mie theory versus geometrical optics: phase function of intensity

Hansen J.E., Travis, L. D. “light scattering in planetary atmospheres”
Space. Sci. Rev. 16, (1974), 527-610

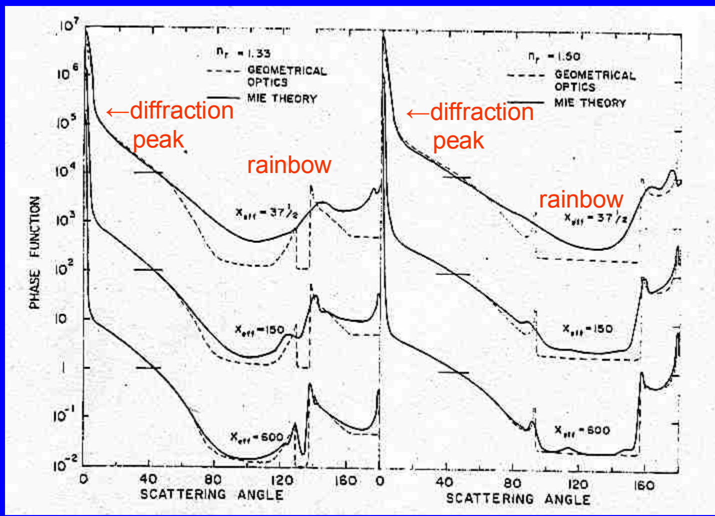

Mie theory versus geometrical optics: phase function of polarization

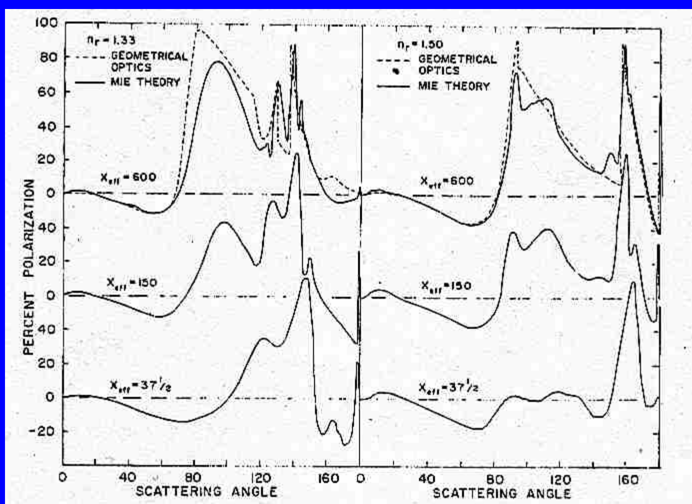

Note that the good agreement in polarization between Mie theory and geometrical optics depends on the particles being perfect spheres. “Rough” spheres differ considerably in their polarization characteristics.

Power law size distributions dn = r^{-a} dr

Mass budget:
a ≥ 4: total dust particle mass resides in the smallest particles.
3 ≤ a < 4: total mass of particles with sizes smaller than a cut-off size is finite.
2 ≤ a < 3: total mass is determined by largest mass. Mass per size range increases with increasing particle size. Small particles insignificant for the mass budget.

Scattered light:

$$\text{Scattered light} \sim \left\{ \begin{array}{c} r^{2-a} \\ r^{6-a} \end{array} \right\} \text{ for } \left\{ \begin{array}{ll} r \gg \lambda: & \sim \text{area} \\ r \ll \lambda: & \text{Rayleigh limit} \end{array} \right\} . \qquad (7)$$

For 2 < a < 6 the contribution of particles of a certain size to the total brightness will asymptotically decrease with increasing as well as with decreasing size. In the Rayleigh limit (r « λ) and in the limit of large particles (r »λ) the scattering efficiency (energy scattered in any direction) does not depend on size.

1. As pointed out by the Halley dust experimenters most of the particle mass resides in the large particles. This is consistent with the idea of the nucleus mass dominating the mass of the coma particles.
2. Rayleigh particles do not significantly contribute to the brightness of scattered light from cometary dust grains. If they did, most of the grain mass would be in the small particles as opposed to item (1).
3. For the size distribution of particles observed in comet Halley the medium size (wavelength size) particles contribute most to the scattered light.
4. Only for a power index $<$ 3 is the scattered light determined by the large particles.

Motion of cometary dust particles under radiation pressure.
Mechanical theory of cometary tails (Bessel and Bredichin).

$$Q_{pr} = Q_{abs} + Q_{sca}(1 - \langle \cos\theta \rangle)$$

$$\beta = \frac{F_R}{F_G} = 0.585 \times 10^{-4} \frac{Q_{pr}}{\rho a}$$

$$F_G = \frac{GM_\odot}{r^2} \left(\tfrac{4}{3}\pi a^3 \rho\right)$$

$$F_R = \frac{Q_{pr}}{c} \left(\frac{L_\odot}{4\pi r^2}\right) \pi a^2$$

Cometary particles are influenced by solar radiation pressure.

From: Fernandez and Jockers, Rep. Progr. Phys. 46, 665-772, 1983

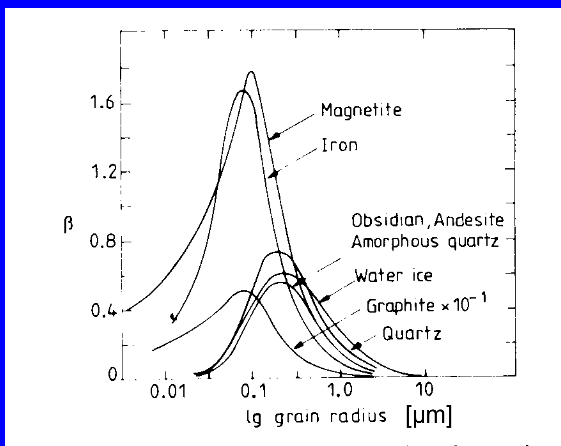

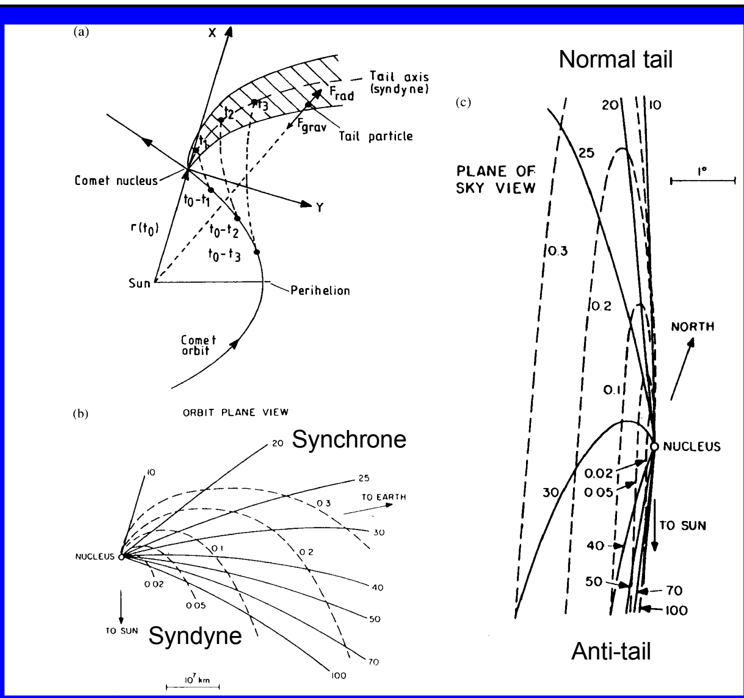

I. de Pater,
J. J. Lissauer,
Planetary Sciences,
Cambridge2001

Synchrone:
Locus of particles of many sizes, emitted from the nucleus at a given time with zero velocity.

Syndyne:
Locus of particles of one size, emitted from the nucleus at all times with zero velocity

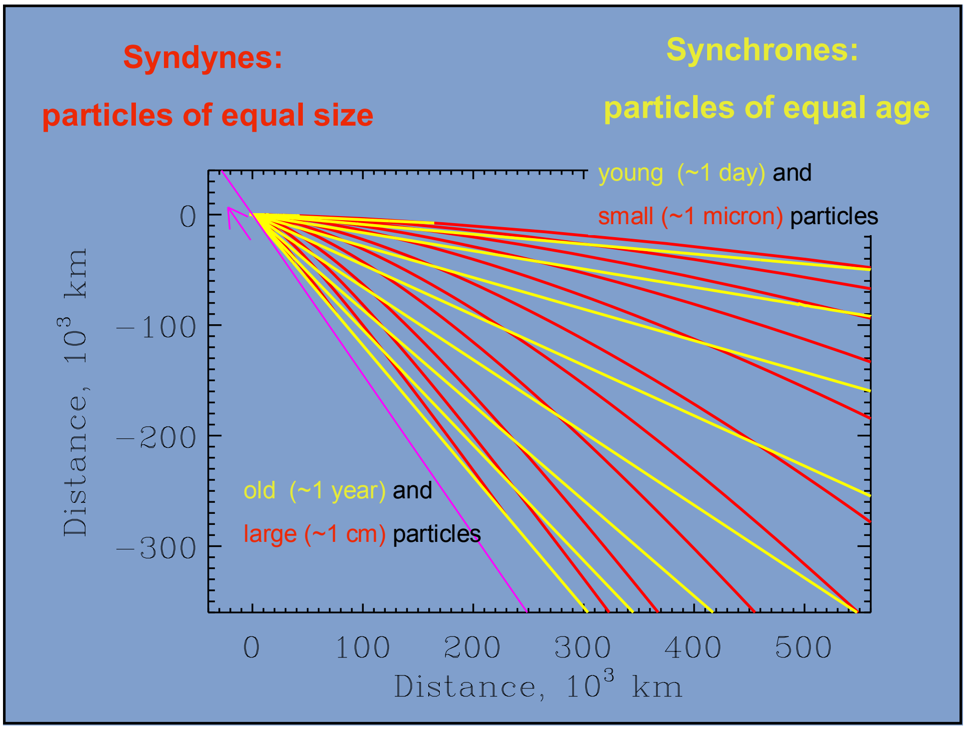
Syndynes:
particles of equal size
Synchrones:
particles of equal age
young (~1 day) and
small (~1 micron) particles
old (~1 year) and
large (~1 cm) particles
Distance, 10³ km
0
−100
−200
−300
0 100 200 300 400 500
Distance, 10³ km

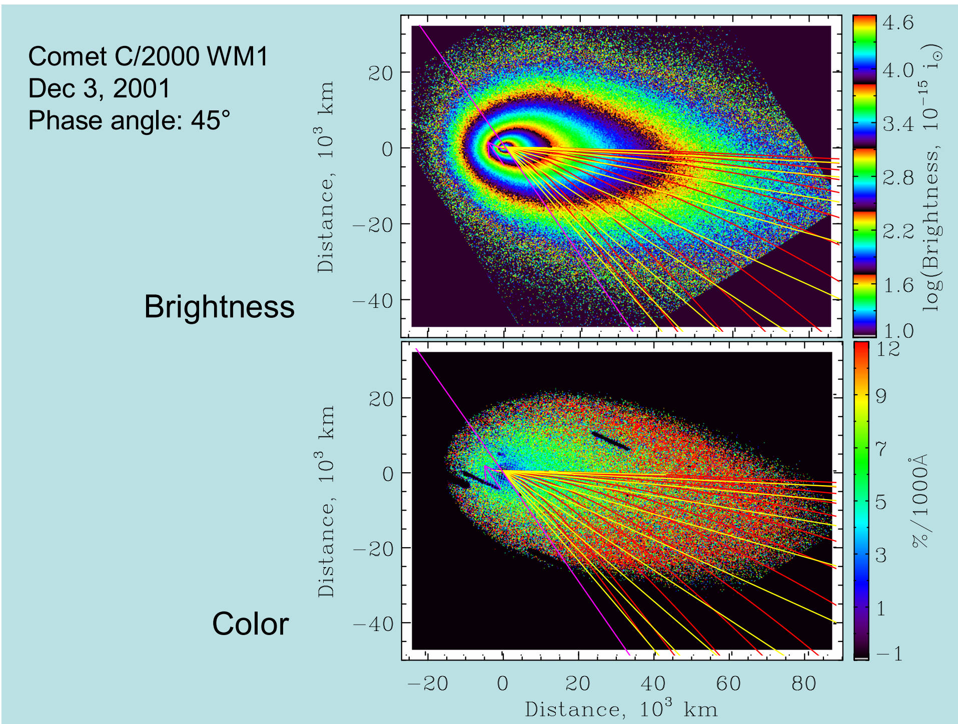
Comet C/2000 WM1
Dec 3, 2001
Phase angle: 45°
Brightness
Color
Distance, 10³ km
20
0
−20
−40
−20 0 20 40 60 80
Distance, 10³ km
4.6
4.0
3.4
2.8
2.2
1.6
1.0
log(Brightness, 10⁻¹⁵ i☉)
12
9
7
5
3
1
−1
%/1000Å

Results of the modeling:

syndynes: $0.001 < \beta = F_R/F_G < 0.5$
corresponding to radii 0.5cm > r > 1μm, if density $\rho = 1$ g cm^{-3},

synchrones: 0.1 < t < 250 days,
maximum velocity = 240 m s^{-1}.

Power law of size distribution $r^{-3.3}$.

Comparison of model and observations

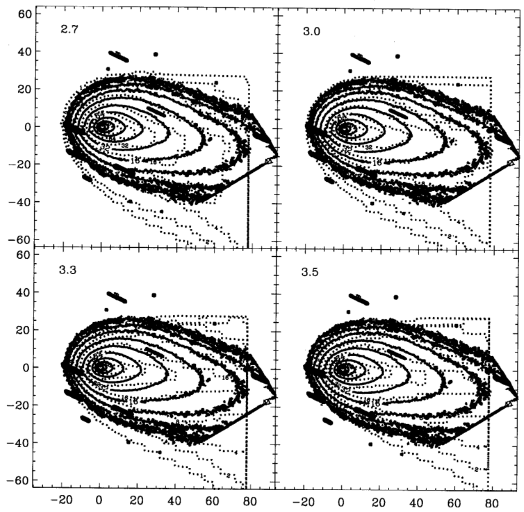

Figure 9: Comparison of the observed continuum image (full line) with the modelled dust distribution. The 4 panels show the result of one Monte Carlo simulation weighted with 4 different particle size distributions.

Antitail of comet Hale-Bopp observed after perihelion, when the Earth passed the comet orbit plane.

Antitails must consist of large particles, as the antitail particles usually were emitted a rather long time ago. If the particles were smaller, they would have been dispersed in the time between ejection and observation. Sometimes we observe a so-called neckline, i. e. particles which were emitted 180˚ earlier in true anomaly. As such particles meet again in the comet plane, the tail is narrow.

(ESO press release)

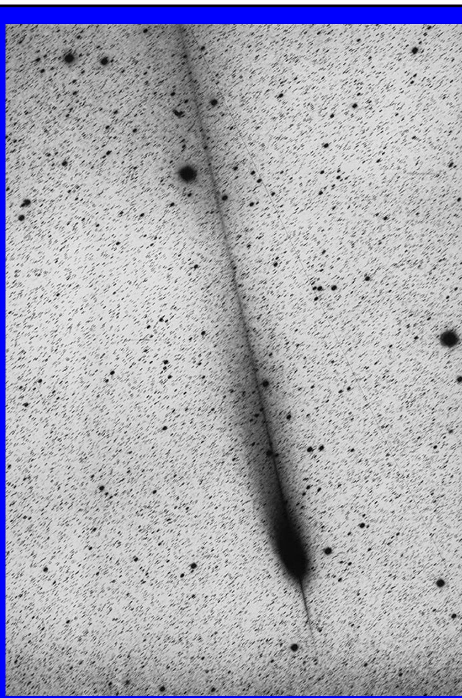

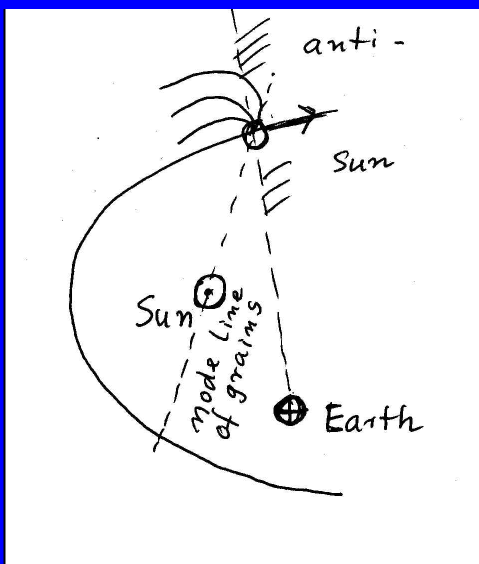

The phase function of brightness of cometary dust grains

θ = 180º - α
θ scattering angle
α phase angle

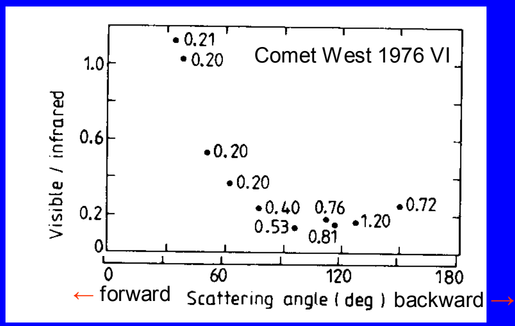

The phase function has a strong forward scattering maximum, a small backward scattering maximum and a minimum at intermediate phase (scattering) angles.

Phase curve obtained from comparison of visual and IR observations (see later).
Data: Comet West 1976 VI.
Ney E. P. and Merrill K.M. Science 194, 1051, 1976.

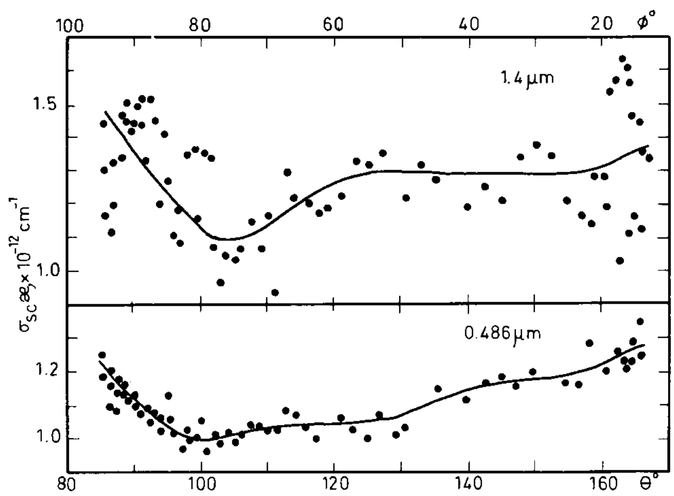

Fig. 4. Phase function of dust scattering at 1.4 μm and 486 nm; σ_{sc} is the volume scattering coefficient at 1000 km from the nucleus in the direction of the Sun and κ is the phase function normalized to 4π. θ is the scattering angle and $\varphi = 180° - \theta$ is the phase angle

Krasnopolsky et al. A&A 187, 707, 1987.

In-situ data of Vega spacecraft at comet Halley.

The phase curve of cometary dust: Observations of comet 96P/Machholz 1 at large phase angle with the SOHO LASCO C3 coronagraph.

Ye. Grynko, K. Jockers, and R. Schwenn, Astron. Astrophys., in press

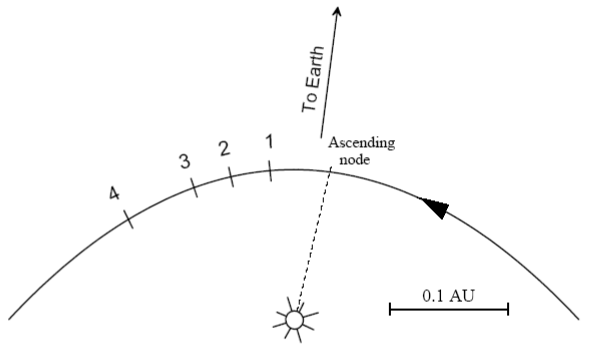

Filter observations:
1. 2002/01/08 22:00 $\alpha = 157^{\circ}$
2. 2002/01/09 10:00 $\alpha = 141^{\circ}$ only intensity
3. 2002/01/09 22:00 $\alpha = 127^{\circ}$
4. 2002/01/10 10:00 $\alpha = 114^{\circ}$ only intensity

Clear glass observations:
40 images from 2002/01/08 $\alpha = 167^{\circ}$
to 2002/01/10 $\alpha = 112^{\circ}$

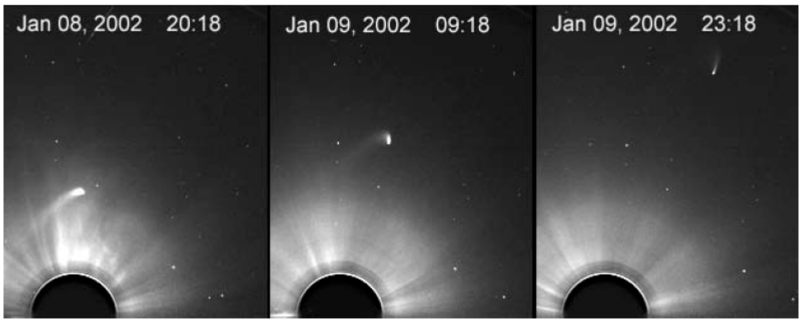

Fig. 3. LASCO C3 images of 96P/Machholz 1 near perihelion.

The forward scattering branch of cometary dust grains

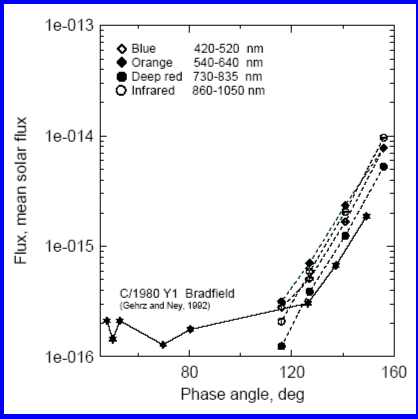

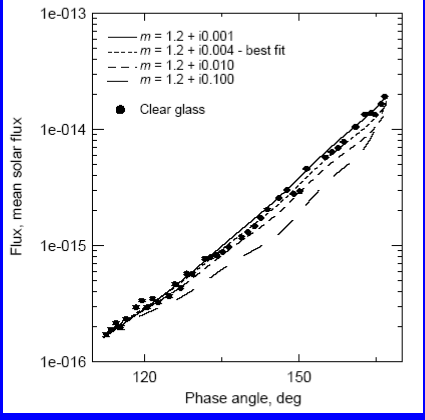

Model fit (Mie theory):
Size distribution ~$r^{-2.5}$,
size range 10 < size parameter $x = 2\pi r/\lambda$ < 400,
with $\lambda \approx$ 0.6 μm size range 1 μm < radius < 40 μm.
Low apparent real part of refractive index caused by porosity of particles.
Note absence of forward diffraction peak.

The backward scattering branch of cometary dust grains

Fig. 4.a–d. Normalized magnitude versus phase angle for **a** P/Halley (data from the present work), where the magnitude is that computed from the continuum window at $\lambda = 5790$ Å ($m_{5790 Å} \approx V$), and only magnitudes measured outside the two "outbursts" have been plotted for clarity; **b** P/Ashbrook-Jackson (data from Kiselev and Chernova, 1981), where the errors of 0.03 mag are as reported in Kiselev and Chernova; **c** Bowell (data from A'Hearn et al., 1984); the errors, where shown, are the errors on log (F_λ) as taken from the original paper; and **d** Stephan-Oterma (data from Millis et al., 1982) where arbitary 0.1 mag errors are plotted. A linear least squares fit for the linear phase coefficient, β, is shown for each comet. All comets are consistent with no opposition effect $\geqq 0.2$ mag for $0° < \alpha < 10°$

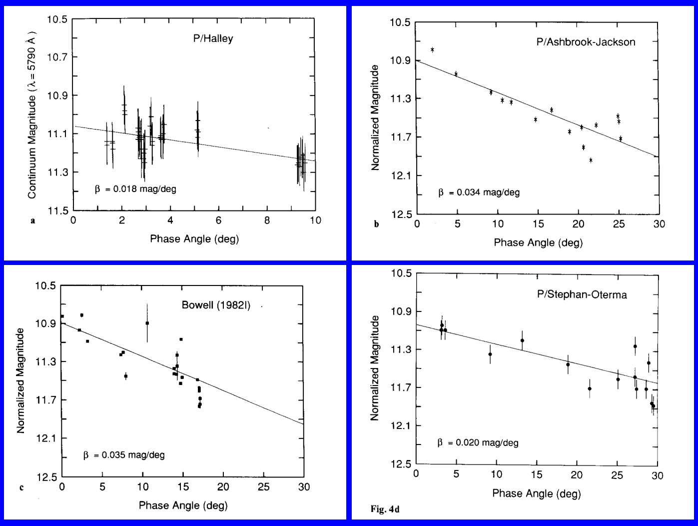

Jewitt D., Meech K. J., Astrophys. J. 310, 937, 1986.

Combining visual and infrared photometry (including silicate peak)

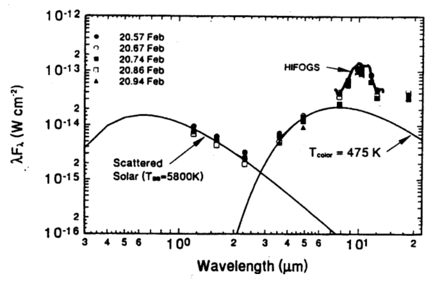

Figure 4. Infrared spectral energy distribution of Hale–Bopp at $r = 1.15$ AU (Williams et al., 1997).

Hanner M.S. et al.:
Thermal emission from the dust coma of comet Hale-Bopp and the composition of the silicate grains.

Earth, Moon and Planets, 79, 247-264, 1997

Overheat: Small particles do not effectively radiate in the IR wavelength range. Particles become hotter than the equilibrium temperature.

Silicate Peak: Particle size dependent. Stronger for small particles.

Gehrz and Ney, Icarus 100, 162, 1992

For a single particle

$$\int_0^\infty \frac{L_{\odot,\lambda}}{4\pi r^2} Q_{\text{abs}}(\lambda, a)\pi a^2 \, d\lambda = \int_0^\infty \pi B[\lambda, T(a,r)] Q_{\text{abs}}(\lambda, a) 4\pi a^2 \, d\lambda$$

Particle may get overheated

$$T = 280/r^{1/2}\ \text{K}$$

For black or grey body

$$F_\lambda = \int_{a_1}^{a_2} \pi B[\lambda, T(a,r)] Q_{\text{abs}}(a,\lambda) a^2 n(a)\, da$$

Particle size distribution

$$A_{\text{bol}} = \frac{Q_{\text{sca}}}{Q_{\text{sca}} + Q_{\text{abs}}}.$$

Scattered/total irradiated

$$E_{\text{tot}} = (\lambda F_\lambda)_{\text{max}} \times 0.74.$$

For Planck curve of any temperature

$$\frac{A_{\text{bol}}}{1 - A_{\text{bol}}} = \frac{Q_{\text{sca}}}{Q_{\text{abs}}} = \frac{(\lambda F_\lambda)_{\text{max vis}}}{(\lambda F_\lambda)_{\text{max IR}}}.$$

Albedo from flux ratio, but phase function must be known

Overheat S = T_{OBS}/T_{BB} is of interest by itself, as it indicates particle size. A further indication for particle size is the existence of silicate emission around 10μm, as this emission occurs only with small particles.

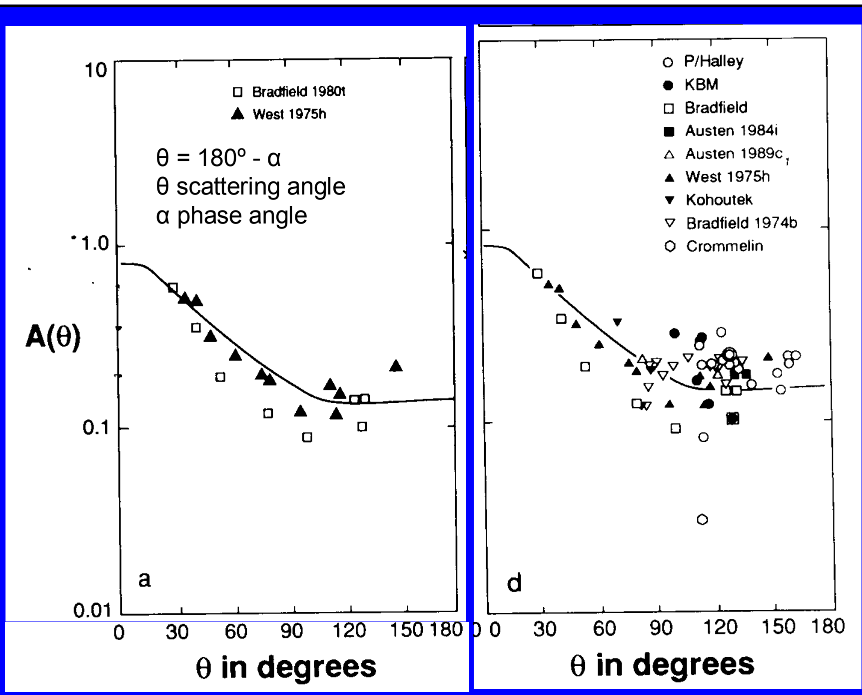

Hanner M.S. et al.: Thermal emission from the dust coma of comet Hale-Bopp and the composition of the silicate grains.

Earth, Moon and Planets, 79, 247-264, 1997

Silicate peak was very strong in comet Hale-Bopp and the particles in this comet are believed to be smaller than average.

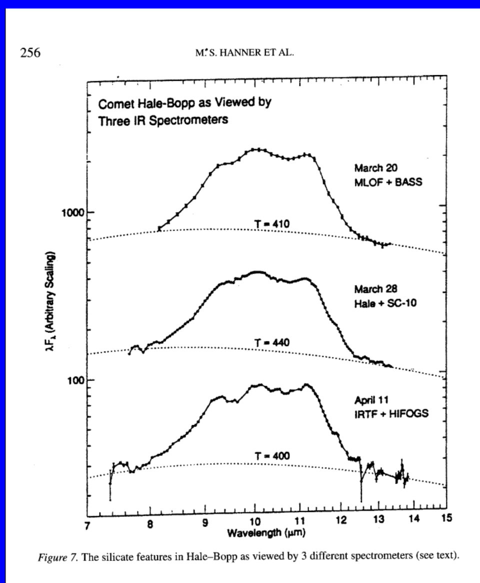

Figure 7. The silicate features in Hale–Bopp as viewed by 3 different spectrometers (see text).

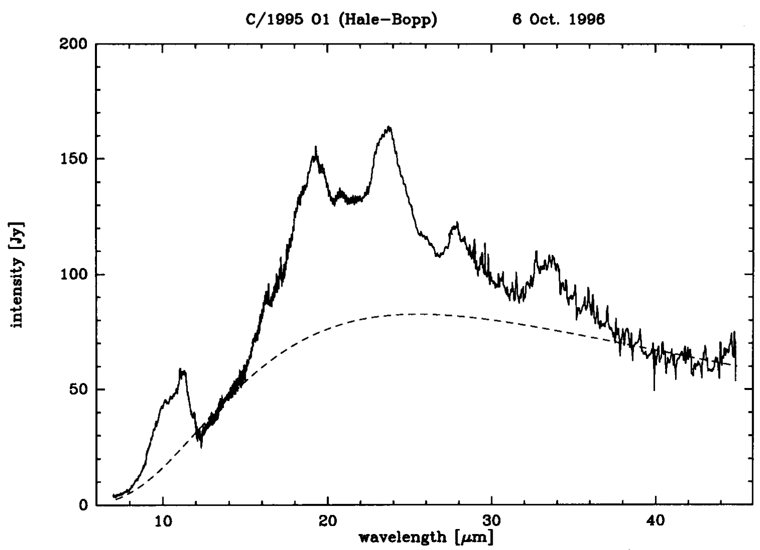

Figure 8. The 7–45 μm spectrum of comet C/1995 O1 (Hale-Bopp) at 2.9 AU from the Sun observed by the short-wavelength spectrometer of *ISO*. The spectral resolution has been degraded to $\lambda/\delta\lambda \sim 500$. The dotted line shows a 200 K black body emission. All spectral features in this region are attributed to Mg-rich crystalline olivine (from [38]).

Crovisier, in Greenberg and Li (eds.) Formation and Evolution of Solids in Space, Kluwer 1999, p. 389.

Mie theory calculations of overheat process

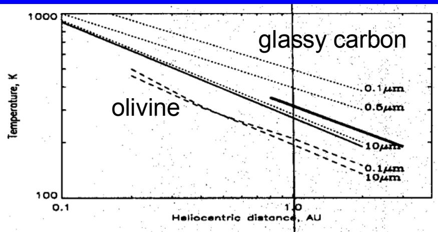

Figure 7. Temperature of a grain versus heliocentric distance. Dotted lines show results for absorptive particles (glassy carbon) of radius 0.1, 0.5, and 10 μm. Dashed lines are for olivine particles of radius 0.1 and 10 μm. The thin solid line is the blackbody temperature. The thick solid line shows the results for comet Halley (*Tokunaga et al.*, 1988). The comet dust temperature is higher than a blackbody, indicating the presence of submicron absorptive particles.

Kolokolova, L., Hanner M.S., Levasseur-Regourd, A., Gustavson, Å.:
Physical properties of cometary dust, to appear in COMETS II, U. of Arizona Press.

Gehrz and Ney,
Icarus 100, 162, 1992

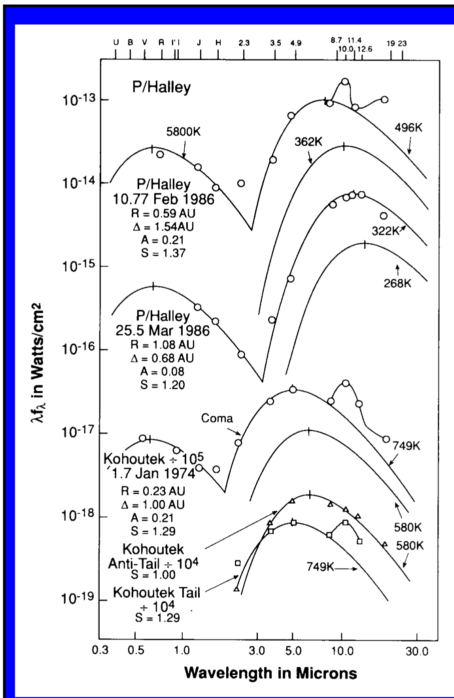

FIG. 1. Typical coma energy distributions for P/Halley when the 10-μm silicate emission feature was present (10.77 February 1986 UT) and absent (25.5 March 1986 UT) showing the scattered solar and thermal continua. Statistical errors are smaller than the plotting symbols. *R* is the heliocentric distance in AU, Δ is the geocentric distance in AU, *A* is the albedo, and *S* is the superheat. The energy distributions of the coma, dust tail, and antitail of Comet Kohoutek are included for comparison (data for Ney 1974a). Also shown are blackbody energy distributions corresponding to the black sphere temperature at the heliocentric distance of each comet as given by Eq. (3).

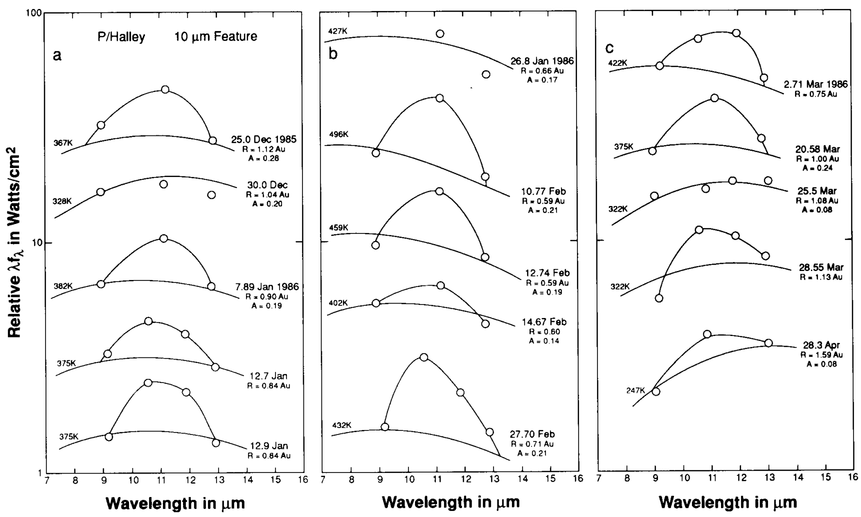

FIG. 3. The 7- to 14-μm energy distribution of P/Halley showing temporal variations observed in the contrast of the 10-μm silicate emissi
feature. *R* and *S* are as defined in Fig. 1. Statistical errors are smaller than the plotting symbols. The silicate feature was occasionally weak
absent for heliocentric distances both less than and larger than 1 AU. On 25.5 March, when the signature was absent, the albedo of P/Halley f
to about 0.08. The blackbody curves were determined from the continuum outside the feature.

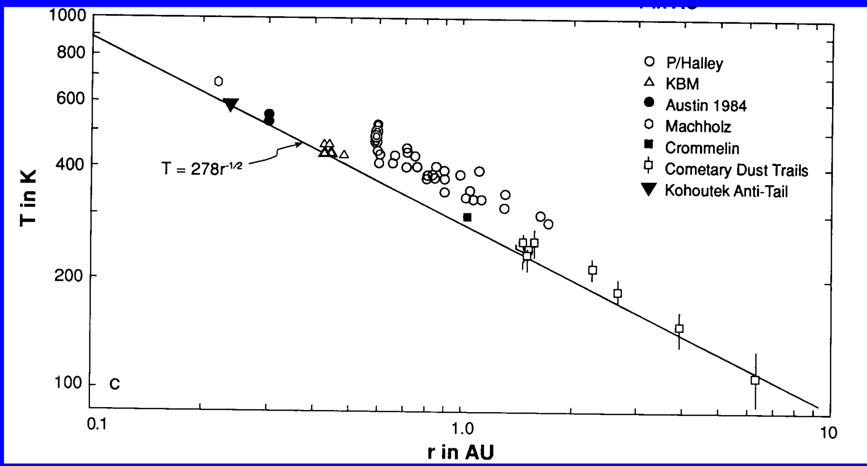

Note low superheat for antitail and dust trails, believed to contain large particles.

Dust trails have been observed in certain short-period comets in the far IR range. These trails are distributed along the orbit of a short-period comet.

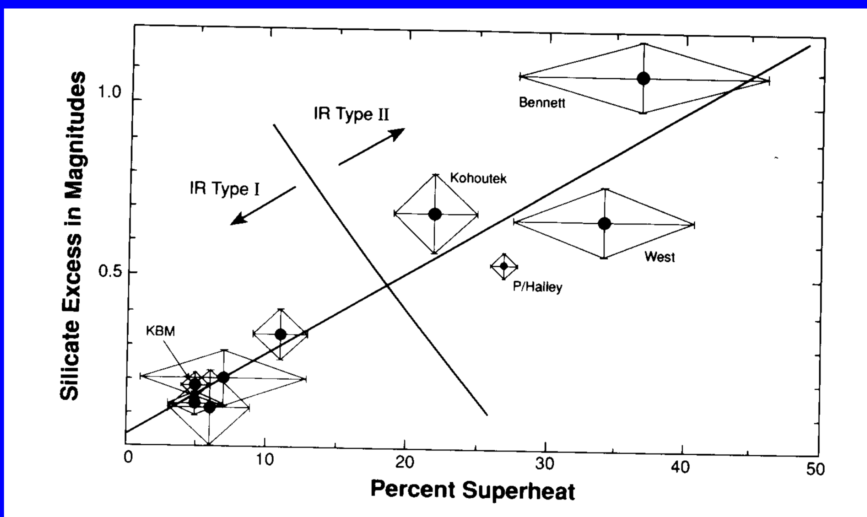

Two types of comets, Type I has the large particles, and Type II the small ones, or perhaps aggregates of small monomers?

TABLE IV
Mean Properties of Selected Bright Comets[1]

NAME	SPECIAL SELECTION CRITERIA, COMMENTS	SILICATE EMISSION EXCESS IN MAGNITUDES	%S (<S>-1 X100)
1975 IX	Extreme IR Type I Comet	0.18 ± 0.03	5 ± 1
1980 XV	IR Type I Comet	0.33 ± 0.07	11 ± 2
1984 XIII	Extreme IR Type I Comet	0.13 ± 0.03	5 ± 2
1985 VIII	IR Type I Comet	0.25	7
$1989c_1$	IR Type I Comet	0.20 ± 0.08	7 ± 6
1989 X	IR Type I Comet	0.11 ± 0.11	6 ± 3
Bennett	Extreme IR Type II Comet	1.08 ± 0.11	37 ± 9
Kohoutek	IR Type II Comet	0.68 ± 0.11	22 ± 3
West	IR Type II Comet	0.66 ± 0.10	34 ± 7
IR Type I	Average over all IR Type Comets above	0.24 ± 0.03	8 ± 1
IR Type II	Average over all IR Type II's above	0.76 ± 0.08	29 ± 3
P/Halley	Average of all days	0.53 ± 0.04	27 ± 1

[1] The errors quoted here are the standard deviation of the mean σ_x, of all measurements of a given comet, or grouping of comets.

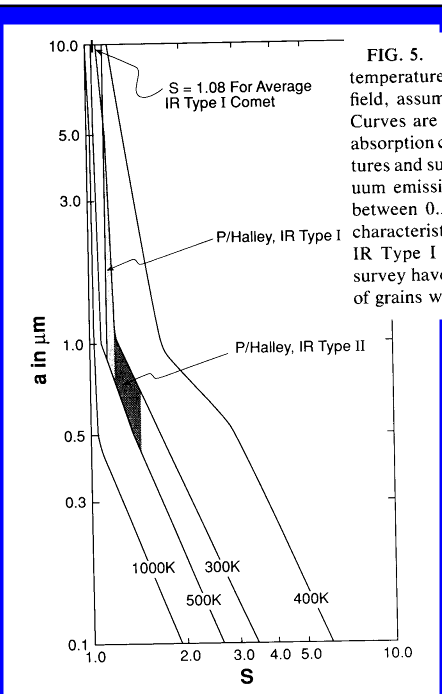

FIG. 5. The superheat S plotted as a function of grain radius a and temperature T_{gr} for small carbon grains illuminated by the solar radiation field, assuming that the Sun has an effective temperature of 5800 K. Curves are based on Gilman's (1974) calculations of the Planck mean absorption cross sections for graphite grains. The range of grain temperatures and superheats recorded for P/Halley confirm that its coma continuum emission was usually produced primarily by particles with radii between 0.5 and 1 micrometer. When P/Halley exhibited IR Type I characteristics, its coma grains may have been as large as 5 μm. Typical IR Type I comets as characterized by the remaining comets in this survey have an average superheat of S = 1.08, suggesting the presence of grains with radii as large as 10 μm.

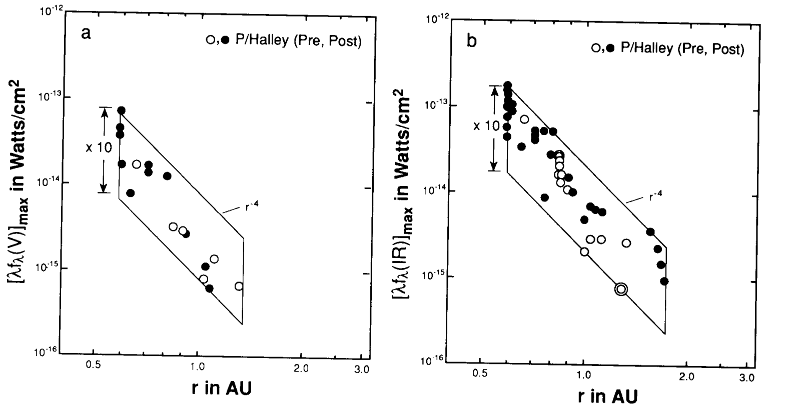

FIG. 7. The activity of the nucleus of P/Halley as a function of heliocentric distance at (a) visible and (b) infrared wavelengths as measured by variations of the apparent intensities $[\lambda f_\lambda(V)]_{max}$ and $[\lambda f_\lambda(IR)]_{max}$, respectively. The coma model described in Appendix A has been used to correct the data for emission in the reference beam and to normalize the apparent intensities to a geocentric distance of $\Delta = 1$ AU and a beam diameter of 20 arcsec. Statistical errors are smaller than the plotting symbols. The parallelograms superimposed on panels (a) and (b) show that P/Halley generally brightened proportionally to r^{-4} as predicted by the theory of nuclear activity described by Eqs. (9) through (12), but varied by almost a factor of 10 on short time scales.

Halleys brightness generally follows the trend of ~ r_h^{-4}, but otherwise is highly variable.

Polarization phase curve of comets

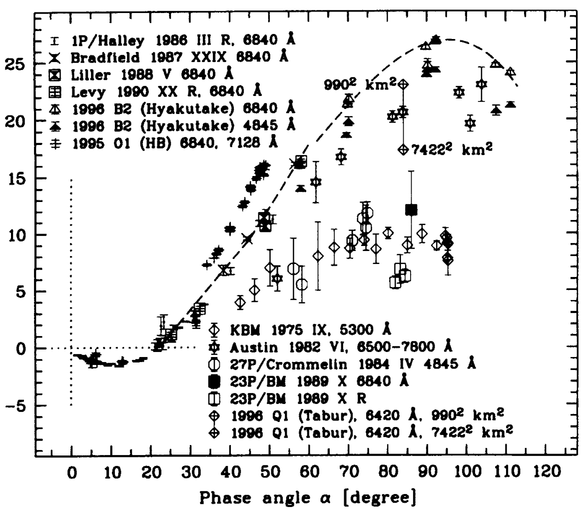

Figure 1. Polarization measurements of the Kiselev group (Dushanbe, Kharkov). The comets listed in the upper left corner are considered dusty, and in the lower right corner gassy. HB = Hale–Bopp, KMB = Kobayashi-Berger-Milon, BM = Brorsen-Metcalf. The dashed line marks the "common" phase curve of the dusty comets. Note the big difference in polarization in comet Brorsen-Metcalf with wide-band R filter (empty squares) and with narrow-band 6840 Å red continuum filter (filled sqare) caused by gas emission transmitted by the R filter. The values for comet 1996 Q1 (Tabur), again a gassy comet, strongly depend on aperture size (crossed diamonds, connected by vertical bar).

Jockers K., Earth, Moon and Planets 79, 221-245, 1997.

Color (wavelength dependent reflectivity of cometary dust grains

$$\frac{\text{reddening}}{100} = \frac{I_R - I_B}{I_R + I_B}\frac{2000}{\lambda_R - \lambda_B} = \frac{10^{0.4(B-R)} - 1}{10^{0.4(B-R)} + 1}\frac{2000}{\lambda_R - \lambda_B}.$$

in the following slides:
work by Jewitt D. and Meech K.J.: 1986, Astrophys. J. 310, 937.
Authors conclude from Mie scattering calculations that the scattering cross-section is dominated by particles that are optically large (a > λ).

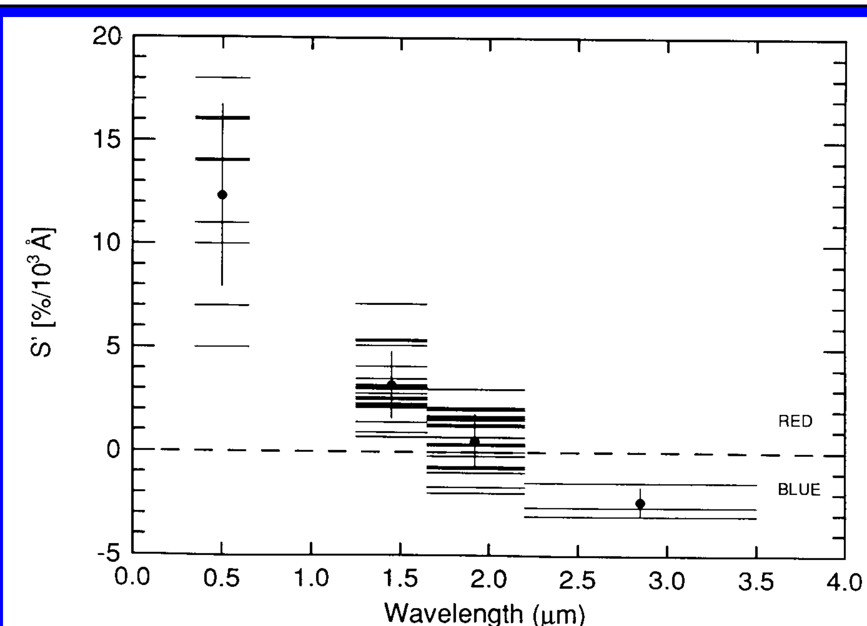

Jewitt D., Meech K. J., Astrophys. J. 310, 937, 1986.

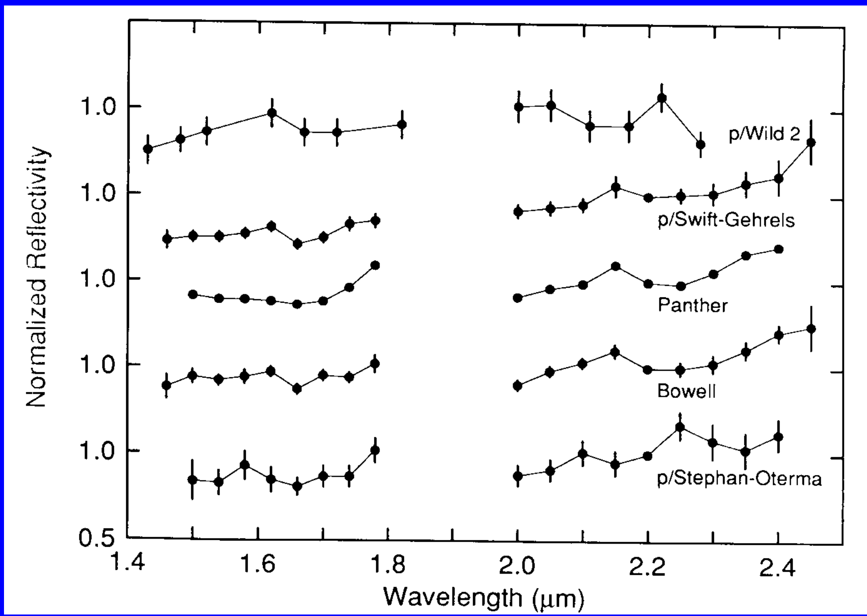

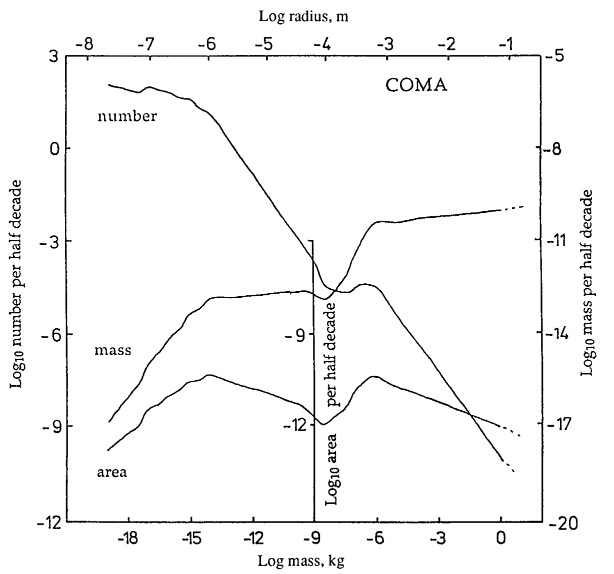

Figure 10. Number, area and mass distributions per cubic meter in the coma are shown, normalized to a distance of 600 km, derived from the Giotto PIA and DIDSY total fluence (McDonnell *et al.*, 1989b).

Spacecraft data of the size distribution of comet Halley's dust.

McDonnel et al, in Newburn et al. (eds.) Comets in the Post-Halley Era, Kluwer 1991.

According to these data very large particles contribute significantly to the brightness.

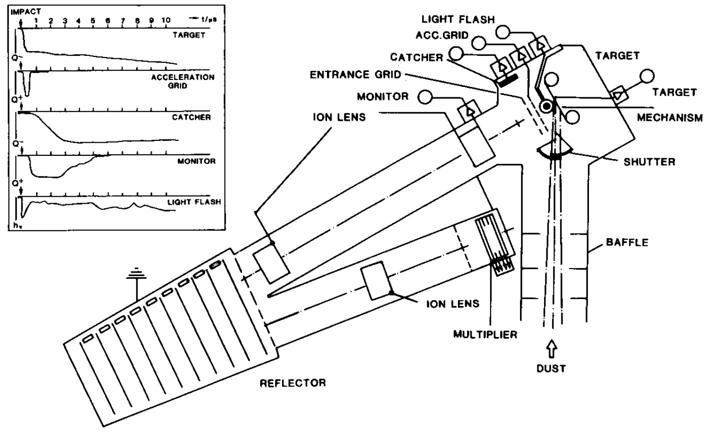

Figure 1. Schematic view of the particulate impact analyzers on board Giotto and VEGAs and 2. The inset shows characteristic front-end signals. From Kissel (1986).

Jessberger E.K., Kissel J., in Newburn et al. (eds.) Comets in the Post-Halley Era, Kluwer 1991, pp. 1075-1092.
Particle impact analyzer: Particles impact on a silver target (upper right), are evaporized and ionized immediately. The ions enter the time of flight system which produces a mass spectrum.

Impact spectra from the Giotto PIA instrument are shown.
Two particle types are illustrated, namely the silicate and carbonaceous CHON classes.
CHON particles consist only of carbon, hydrogen, oxygen and nitrogen.

The comet's total content of organic material was higher than the mineral content by a factor 3-10.

Spectra from
McDonnel et al., in Newburn et al. (eds.) Comets in the Post-Halley Era, Kluwer 1991, pp 1043-1073

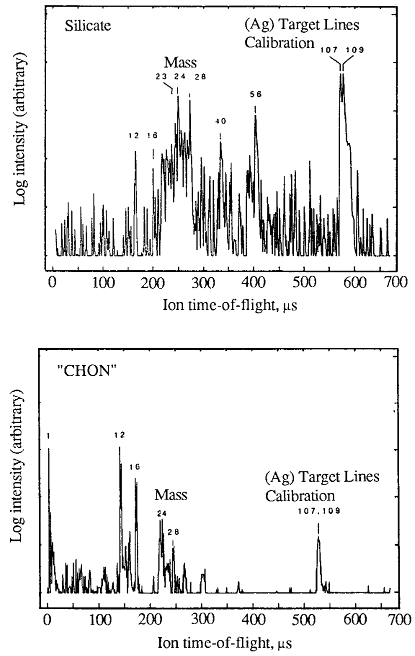

Martha S. Hanner and
Thomas L. Hayward,
Infrared observations of comet 81P/Wild 2 in 1997, 2003
Icarus 161, 164-173

Comet 81P/Wild 2displayed a 10-µm silicate feature about 20% above continuum.

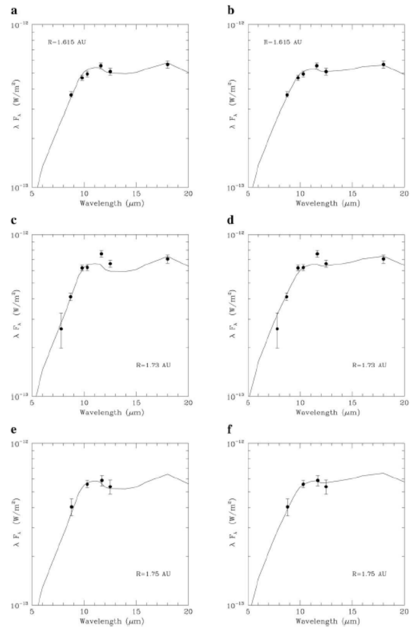

Fig. 3. P/Wild 2 spectral energy distribution compared with best-fit thermal models for the two size distributions described in the text. (a) Apr. 4, S–H $n(a)$; (b) Apr. 4, GIOTTO $n(a)$; (c) Feb. 24, S–H $n(a)$; (d) Feb. 24, GIOTTO $n(a)$; (e) Feb. 20, S–H $n(a)$; (f) Feb. 20, GIOTTO $n(a)$.

Dust composition measurements in comet 81P/Wild 2 with CIDA (Cometary and Interstellar Dust Analyzer)

In contrast to measurements in comet 2P/Halley negative ions were measured as well.

Because of the low encounter speed of 6 kms^{-1} organic compounds are much better preserved than they were in comet 1P/Halley. But in 81P not the whole particle is destroyed and the ions come from the outer layers of the particle.

The 29 spectra obtained during the flyby of Comet 81P/Wild 2 confirm the predominance of organic matter. In moving from interstellar to cometary dust, the organic material seems to lose most of its hydrogen and oxygen as water and carbon monoxide. These are now present in the comet as gas phases, whereas the dust is rich in nitrogen-containing species. No traces of amino acids were found.

Kissel et al., The cometary and interstellar dust analyzer at comet 81P/Wild 2, 2004, Science 304, 1774-1776.

CIDA positive ion spectrum measured in the coma of comet 81P/Wild 2

1. Three spectra like Fig. 1 →
CH^+ + traces of N^+, NH^+, O^+, OH^+
N-heterocyclic fragment ions,
$C_3NH_x^+$ (x=2, 4, 6, 8).
no complex O-containing species

2. Na^+, K^+ (contaminants of Ar target), $C_6NH_4^+$ (H2- loss from $C_6NH_6^+$), abundance of heterocyclic, probably annealed rings as backbones of most of the organic structure

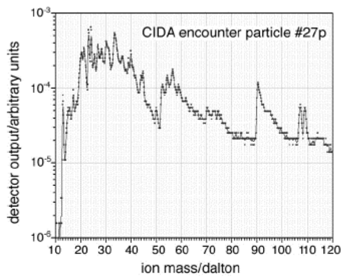

Fig. 1. A positive-ion spectrum, converted from time of flight into a linear mass scale. The amplitude scale is logarithmic. The spectrum is typical for nitrogen organic chemistry. The *m/z* = 107, 109 doublet is due to the Ag^+ from the target.

Negative ion spectra from comet 81P Wild 2 (Fig. 2) and from 3 interstellar particles (Fig. 3)

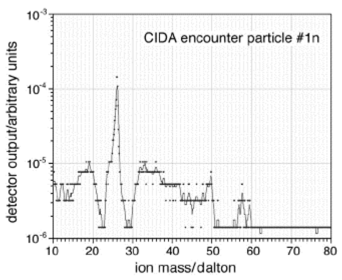

Fig. 2. A negative-ion spectrum, converted like Fig. 1. The dominating ion is CN^-, as is typical for nitrogen organic chemistry. The oxygen region (*m/z* = 16, 17) is surprisingly low; however, the SH^- (*m/z* = 33, 35) is high. The shift of the H^- line is a known instrumental effect.

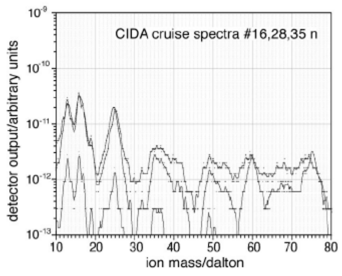

Fig. 3. Three negative-ion spectra, converted like Fig. 2, are shown for comparison with Fig. 2. The spectra are from three interstellar dust particles. The carbon-oxygen region is dominant, and the major peak in the mass range from 20 to 30 daltons is clearly 25, not 26.

Crovisier, in Greenberg and Li (eds.) Formation and Evolution of Solids in Space, Kluwer 1999, p. 389.

Note N deficiency in comets.

TABLE 8. The elemental composition of comets. Average elemental abundances measured in comet C/1965 S1 (Ikeya-Seki) (from [7]), in Halley's dust grains and in the whole comet dust and volatiles (from [67]), and in other solar system objects (from [5]). The abundances are normalized to Mg (to the solar system abundance of Fe for Ikeya-Seki, in which Mg was not observed).

element	Ikeya-Seki[a)]	P/Halley		Solar system	CI-chondrite
		dust	dust + ice		
H		2 025.	4 062.	2.6×10^{6}	492.
Li	†			0.0053	0.0053
C		814.	1 010.	0.	70.5
N		42.	95.	291.	5.6
O		890.	2 040.	2 216.	712.
Na	†	10.	10.	5.3	5.3
Mg	(=100.0)	=100.0	=100.0	=100.0	=100.0
Al		6.8	6.8	7.9	7.9
Si		185.	185.	93.	93.
P				1.0	1.0
S		72.	72.	48.	48.
K	†	0.2	0.2	0.35	0.35
Ca		6.3	6.3	5.7	5.7
Ti	<0.02	0.4	0.4	0.22	0.22
V	0.01			0.027	0.027
Cr	0.08	0.9	0.9	1.3	1.3
Mn	0.5	0.5	0.5	0.89	0.89
Fe	84.	52.	52.	84.	84.
Co	0.4	0.3	0.3	0.21	0.21
Ni	7.2	4.1	4.1	4.6	4.6
Cu	0.2			0.049	0.049

) In addition, abundances relative to Na were determined to be 1.6×10^{-3} for K and $< 2.5\times10^{-5}$ for Li [90].